JOURNAL OF MATERIAL SCIENCE 33 (1998) 3665–3669

Microstructure and magnetic properties of Ni–Zn ferrites

M. I. ROSALES*, M. P. CUAUTLE
Instituto de Investigaciones Eléctricas, Depto. de Materiales, Apartado Postal 1-475, Cuernavaca, Mor. 62001, México
V. M. CASTAÑO
Instituto de Física, UNAM, Apartado Postal 20-364, México D.F. 01000, México

Ni–Zn ferrites were prepared in air by using the conventional ceramic powder methodology. The compositions analysed belong to the type $Ni_xZn_{1-x}Fe_2O_4$ ferrites, with x ranging from 0.3–0.4. Copper wire was coiled round the specimens, previously pressed to a toroidal shape, to characterize their magnetic properties as a function of the frequency of the applied electric field. Powder X-ray diffraction, scanning electron microscopy and microanalysis, and the magnetic susceptibility of the ferrites, were studied, indicating that the highest permeability is achieved at the composition $x=0.3$, a result which is correlated to the microstructural characterization. The Curie temperature was also determined to range from 60–130 °C, depending on the specific composition.

1. Introduction

Among the magnetic materials, the so-called soft ferrites today represent not only an active field of research and development [1–8], but also an important commercial activity. Indeed, owing to their very high electrical resistivity (over one million times that of equivalent magnetic alloys) which implies low losses due to parasitic currents, and to their susceptibility, soft ferrites are preferred in applications ranging from transformers to magnetic heads. In addition, their high permeability in the r.f. frequency region, make polycrystalline ferrites suitable for an increasing number of electronic devices. Generally speaking, most soft ferrites in practical use have the composition $MOFe_2O_3$ (where M represents a divalent ion) and present the spinel ($MgAl_2O_4$) structure in which the oxygen atoms form a close-packed f c c structure. It is known, however, that the compounds capable of crystallizing in the spinel system, can present either of two structures: the normal spinel or the inverse spinel. In the normal spinel (such as $ZnFe_2O_4$ ferrite), the metallic ions M^{2+} are located in the tetrahedral sites, symmetrically surrounded by four O^{2-} ions. In the inverse spinel (like $NiFe_2O_4$ ferrite), half of the Fe^{3+} ions are located in the tetrahedral positions which Mg^{2+} ions occupy in the original spinel structure, whereas the other half, along with all the Ni^{2+} ions, are in the octahedral positions which the Al^{3+} occupy in the original spinel structure. Therefore, a normal ferrite can be described as $M^{2+}Fe_2^{3+}O_4$ and an inverse ferrite as $Fe^{3+}(M^{2+}, Fe^{3+})O_4$.

This is of great relevance because one of the most popular magnetic materials studied and employed nowadays is precisely the Ni–Zn ferrite, which is a material consisting of a combination of normal and inverse spinels which has very important magnetic properties for applications above 1 MHz [8–11], and despite the progress in the basic science, the scientific aspects of the industrial processing of soft ferrites still pose some important questions, especially in the area of how the processing conditions influence the microstructure and how the microstructure affects the performance. Moreover, it is an accepted fact that many of the relevant electromagnetic characteristics of ferrite materials depend strongly on the microstructure of the fired body [10–12]. Accordingly, in this paper, a study of the evolution of the microstructure of Ni–Zn ferrites, prepared by the standard procedure reported in the literature [11–14] is presented, along with a correlation with the corresponding magnetic properties of these materials.

2. Experimental procedure

2.1. Materials and preparation procedure

NiO (Baker, 99% purity), ZnO (Baker, 99.6%) and Fe_2O_3 (Baker, 99.6%) powders were employed as raw materials. Table I contains a summary of the nine sets

* *Present address*: Centro de Investigación en Materiales Avanzados (CIMAV), Miguel de Cervantes 120, Complejo Industrial Chihuahua, 31110 Chihuahua, Chihuahua, México.

TABLE I Composition and preparation conditions

Sample	Nominal composition	Sintering conditions
A	$Ni_{0.3}Zn_{0.7}Fe_2O_4$	1150 °C, 12 h
B	$Ni_{0.4}Zn_{0.6}Fe_2O_4$	2.41 min^{-1} air flux
C	$Ni_{0.35}Zn_{0.65}Fe_2O_4$	
D	$Ni_{0.3}Zn_{0.7}Fe_2O_4$	1150 °C, 6, 12, 24, 96 h
E	$Ni_{0.4}Zn_{0.6}Fe_2O_4$	1.41 min^{-1} air flux
F	$Ni_{0.35}Zn_{0.65}Fe_2O_4$	
G	$Ni_{0.3}Zn_{0.7}Fe_2O_4$	1150 °C, 6, 12, 24, 48, 96 h
H	$Ni_{0.4}\ Zn_{0.6}\ Fe_2O_4$	2.41 min^{-1} air flux
I	$Ni_{0.35}\ Zn_{0.65}\ Fe_2O_4$	

or families of samples prepared. As observed, each family consists of the same $(NiO)_x(ZnO)_{1-x}$ composition, but with different sintering procedures, as will be established below. In this way, both composition and sintering conditions could be explored in terms of their influence on the final magnetic properties. The oxides were mixed and milled for various compositions (Table I) in a ball mill for 6 h, with 50 wt% ethanol. Then, the resulting paste was dried at 70 °C for 8 h under room conditions. Polyvinyl alcohol was added at 2.5 wt% to plastify the specimens, which were then milled again for 8 h in a ball mill. The resulting powders were then sieved (300 mesh) and pressed, at 1.1 ton cm^{-2} for 3 min into a toroidal shape with 2.3 cm inner diameter, 3.7 cm external diameter and 0.8 cm thickness.

Finally, different sintering procedures were followed (Table I), for samples within each family of specimens prepared. In each case, the heating rate was as follows:

$$\text{room temperature} \rightarrow 400\,^{\circ}\text{C}, \quad 3\,\text{h}$$

$$400\,^{\circ}\text{C} \rightarrow 1150\,^{\circ}\text{C}, \quad 4\,\text{h}$$

$$1150\,^{\circ}\text{C} \rightarrow 1150\,^{\circ}\text{C}, \quad x\,\text{h}$$

where x was 6, 12, 24, 48 and 96 h, depending on the specific case.

2.2. Characterization techniques

X-ray powder diffraction was carried out in a Siemens D-5000 machine with CuK_α radiation and at 2 deg s^{-1} scanning rate. Density was evaluated by the mass/volume relation method in carefully polished samples. Scanning electron microscopy was performed in a Zeiss DSM-960 microscope with a secondary electron detector, equipped with a Kevex Delta-4 microanalysis attachment, at 25 KeV. Magnetic susceptibility, inductance, quality factor and magnetic losses were measured as a function of frequency in an impedance bridge (HP-4192) in the range from 5 Hz to 13 MHz, in toroidal samples, coiled with copper 25 calibre wire, with six turns around the toroid. The Curie temperature was evaluated in each case by using the experimental arrangement shown schematically in Fig. 1, which is a design especially meant for measuring the initial magnetic permeability as a function of temperature, with good accuracy [15]. This is extremely important, because at the Curie point, the initial permeability falls from its maximum value to almost zero, making the measurement difficult with the standard procedures reported before. The number of turns in the primary coil of the transformer was 10 and 5 in the secondary, with a current in the primary of 0.01 mA at 10 kHz.

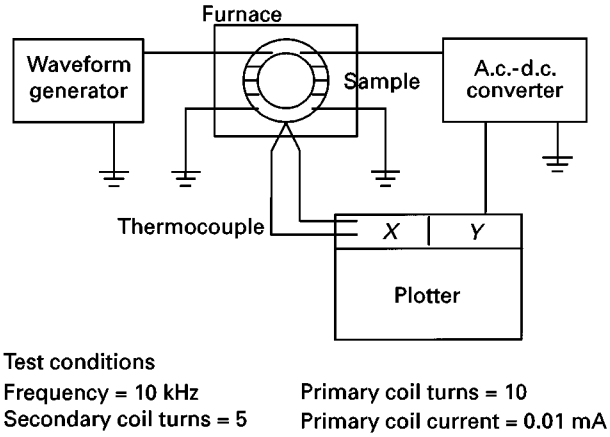

Figure 1 Experimental arrangement for measuring the Curie temperature, T_c, of the samples.

TABLE II Properties of samples A, B and C

Sample	Density (g cm^{-3})	μ	T_c (°C)	x
A	5.06	2360	59	0.297
B	5.06	81	125	0.3486
C	5.013	1196	86	0.3439

TABLE III Properties of samples D, E and F

Sample	Sintering time (h)	Density (g cm^{-3})	μ	T_c (°C)	x
D	6	5.01	827	61	0.2936
	12	5.08	925	62	0.2956
	24	5.23	975	65	0.3107
	96	5.23	1061	69	0.3389
E	6	5.1	873	132	0.3904
	12	5.14	953	134	0.3943
	24	5.19	955	138	0.4207
	96	5.21	1036	136	0.4347
F	6	5.03	1246	105	0.3451
	12	5.1	1440	98	0.3443
	24	5.13	1661	92	0.3863
	96	5.2	1768	104	0.4021

3. Results and discussion

Table II contains a summary of some of the properties measured in the families of samples A, B and C, that is, samples with different composition, but subjected to the same sintering conditions. It is interesting to note the homogeneity of the final specimens, in terms of their corresponding densities, within each group. Also, samples of composition A showed the highest susceptibility (with exception of family G, which will be discussed later), which is over 30 times bigger than that of samples of family B. Tables III and IV contain

TABLE IV Properties of samples G, H and I

Sample	Sintering time (h)	Density (g cm^{-3})	μ	T_c (°C)	x
G	6	5	1740	59	0.313
	12	5.15	2610	60	0.3168
	24	5.23	2926	60	0.3165
	48	5.21	3380	62	0.3177
	96	5.22	3422	63	0.3291
H	6	5.06	884	126	0.3947
	12	5.08	941	130	0.4092
	24	5.2	1073	132	0.4098
	48	5.22	1120	140	0.427
	96	5.24	1202	135	0.4337
I	6	5.15	1337	91	0.364
	12	5.17	1617	94	0.3676
	24	5.2	1870	96	0.3793
	48	5.2	1830	99	0.3801
	96	5.2	1665	97	0.3937

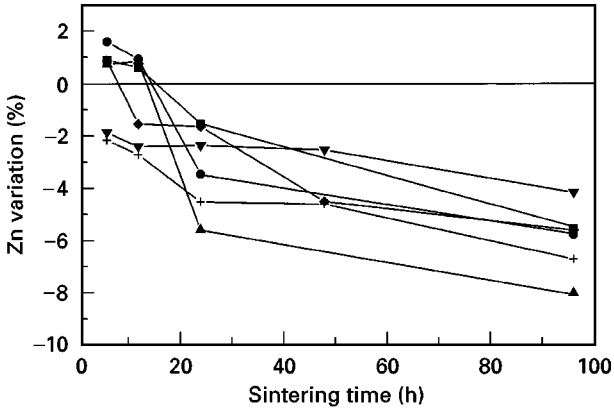

Figure 2 Zinc loss as a function of sintering time for families D–I. (■) D, (●) E, (▲) F, (▼) G, (◆) H, (+) I.

the results of the corresponding characterization of the other sets of samples specified in Table I. As observed there, a more extended and complete sintering procedure implies, as expected, a higher density of the materials. However, this is not necessarily reflected in the permeability, that is, on the magnetic properties of the ferrites prepared. In all cases analysed, regardless of the sintering conditions employed, the composition $Ni_xZn_{1-x}Fe_2O_4$ with $x = 0.3$ always corresponded to the highest permeability. In fact, the highest permeability attained, including all the specimens prepared, corresponds to the family identified as G, which corresponds to the nominal composition $x = 0.3$, with a relatively long sintering period. In this case, it is interesting to note that, after 40 h heat treatment, no significant improvement in the permeability is measured. However, the longer the sintering, the higher was the density, even for the samples without the optimal composition. Thus, for the range of compositions prepared, there exists a specific stoichiometry for the Ni–Zn ferrite system for which, whatever the preparation procedure in terms of the sintering route followed, the magnetic permeability is the best possible. This probably has to do with the solid-state solubility limits of the oxides employed, an area poorly explored in magnetic materials and which certainly deserves more attention, because the segregation phenomena and grain-size distribution, known to affect the magnetic performance of the ferrites, are related to the diffusion and to the solid solution-forming capabilities of the oxides involved. Fig. 2 shows zinc content variation as a function of sintering time. An important increase can be observed in zinc losses as the sintering time increases.

As mentioned, zinc ferrites form a normal spinel structure, where the metal ions are found in the tetrahedral sites, surrounded by four O^{2-} ions. In the inverse spinel structure, which is the case of the nickel ferrite, half of the total Fe^{3+} ions are located in the tetrahedral positions, whereas the other half, along with all the Ni^{2+} ions, are in the octahedral sites. In the case of a Ni–Zn ferrite, the situation can be more or less understood, because it has been demonstrated [16, 17], that in many solid solutions, the zinc ions occupy the tetrahedral positions and the energy threshold for driving them into octahedral sites is rather high. Moreover, recent EXAFS studies [18] have corroborated that in Ni–Zn ferrites, zinc ions occupy the tetrahedral sites and the iron cations occupy both sites in a ratio determined by the Zn/Fe ratio. Therefore, because the nickel ions occupy the octahedral positions, an overall excess of Fe_2O_3 in the Ni–Zn ferrite is produced, which can be dissolved into the spinel phase by the magnetite-forming reaction

$$3Fe_2O_3 \rightleftharpoons 2FeFe_2O_4 + \tfrac{1}{2}\,O_2 \qquad (1)$$

With this mechanism, the magnetite phase can form solid solutions with most of ferrites. According to this model, a slight excess of NiO would drive the final compound away from the solid-solution condition, to a state where no adequate dissolution can be achieved, thus producing an abrupt fall in the magnetic performance, as was indeed experimentally observed. Accordingly, we are proposing the detailed control of NiO in these ferrites, as a tool for controlling the magnetic performance of these materials, as will be seen below.

On the other hand, it has been found [9] that the mean grain size is the controlling parameter for the magnetic susceptibility of spinel $NiFe_2O_4$ materials. According to our results, not only is the average grain size directly correlated to the permeability of a given sample in the Ni–Zn ferrites, but also to the grain-size distribution. Fig. 3 shows the mean grain size, as observed by SEM. As has been determined in the case of Mn–Zn ferrites [12], for Ni–Zn ferrites the grain-size distribution, the sharpness of the grain boundaries, as well as the local deviations from stoichiometry, seem to be also a finer probe for the microstructure–magnetism relationships. Indeed, Table II–IV show a summary of the results of the microanalysis (x in $Ni_xZn_{1-x}Fe_2O_4$) for all the families of samples, indicating that the best specimens, in terms of the susceptibilities attained, are those with the highest homogeneity at a microscopic level, which also gives a clue to the segregation characteristics of each composition. The higher deviations from the nominal stoichiometry, take place precisely at value of

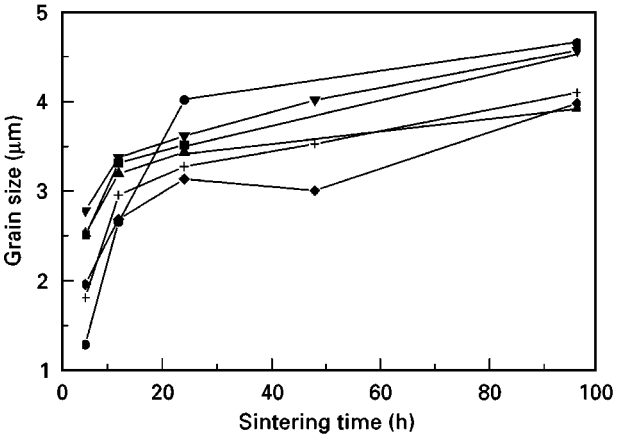

Figure 3 Mean grain size as a function of sintering time for families D–I. (■) D, (●) E, (▲) F, (▼) G, (◆) H, (+) I.

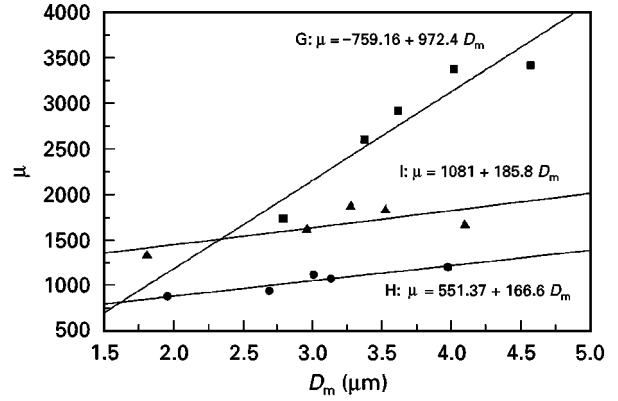

Figure 4 Permeability versus mean grain size, D_m, for families G–I.

x further away from the optimal value of $x = 0.3$, which could also provide some insight into the solubility limits.

Fig. 4 contains a plot of the initial magnetic permeability, μ, at 1 kHz as a function of the mean grain size. By applying a least squares fitting to the experimental data, a straight line can be drawn, as shown in the figure, for the whole range of compositions studied. These results indicate that the grain size in the solid solution of the Ni–Zn ferrites constitutes a way of estimating the magnetic permeability of the oxide mixtures. In this figure, it is important to notice the increase of the slope as the nickel content decreases.

It has been found that the saturation magnetization in ferrites depends on the pore volume and on the volume occupied by non-magnetic inclusions [19]. Thus, one possible way to predict the magnetic performance of the Ni–Zn ferrites studied would be through the following empirical expression

$$\mu_{eff} = \mu_t(1 - V_{pi}) \quad (2)$$

where μ_{eff} is the effective permeability, μ_t the theoretical permeability of a single-crystal material, and V_{pi} is the volume fraction occupied by pores and for non-magnetic inclusions, such as impurities or glassy interfaces, which have been observed strongly to affect the magnetic properties in similar materials [12]. Evaluation of V_{pi} can be achieved through various approaches, either from X-ray or microscopic analysis or from the density of the material. Indeed, as can be noticed in Tables II–IV, for a given composition, that the change in density is related to the corresponding permeability of the material.

Finally, for the results of the Curie temperature measurements for all compositions prepared, a least squares fitting allows, as a crude approximation, extrapolation of the expected value which a pure nickel ferrite would have. The extrapolation provides a figure of $T_C = 575\,^{\circ}C$, whereas the reported experimental value is $T_C = 585\,^{\circ}C$, which constitutes a remarkable agreement. This result is further evidence of the relevance of the Ni/Zn relation, and the corresponding solubility and segregation behaviour, on the magnetic properties of Ni–Zn ferrites.

4. Conclusions

The nickel content in Ni–Zn ferrites plays an important role on the magnetic performance of these materials. The specific solubility and segregation behaviour in these complex solid solutions of normal and inverse spinels deserves further investigation. A numerical relation was established for the permeability function on the grain size for all the compositions prepared. A decreasing slope is observed as the nickel content increases.

A crude numerical extrapolation of the Curie temperature to the hypothetical case of a pure nickel ferrite was remarkably good. Inductance spectroscopy studies [20–22] have been reported separately [23], aiming to provide clues to the different polarization mechanisms taking place in these materials for each nickel composition. Finally, the scientific details of the processing conditions are beginning to be taken into account in the development of improved soft ferrites, to the extent that novel powder metallurgy methods using warm compaction and polymer coating of the iron particles [24] have been able to achieve excellent structural properties and remarkable magnetic performance, indicating that the type of results found in this present work are correctly aimed towards the production of adequate magnetic materials.

Acknowledgement

The authors are indebted to Dr Victor Salinas for his technical support for the microanalysis.

References

1. T. Y. TSENG and J. C. LIN, *J. Mater. Sci. Lett.* **8** (1989) 261.
2. *Idem.*, *IEEE Trans. Mag.* **25** (1989) 4405.
3. U. VARSHNEY and R. K. PURI, *ibid.* **25** (1989) 3109.
4. U. VARSHNEY, R. K. PURI, K. H. RAO and R. G. MENDIRATTA, in "Ferrites, Proceedings of **ICF-3**" (1981) p. 207.
5. R. K. PURI and U. VARSHNEY, *J. Phys. Chem. Solids* **44** (1983) 655.
6. S. FISCHER, C. MICHALK, W. TÖPELMANN and H. SCHELER, *Ceram. Int.* **18** (1992) 317.
7. F. G. STICKLAND, *J. Phys. Chem.* **67** (1963) 2504.

8. V. V. ZAPOROZHETS and V. V. OLEYNIK, *Fiz. Metal Metalloved*, **61** (1986) 192.
9. J. GIERALTOWSKI and A. GLOBUS, *IEEE Trans. Mag.* **MAG-13** (1977) 1357.
10. M. I. ROSALES, PhD Progress Report, UNAM, Mexico City (1995).
11. Y. YAMATO and A. MAKINO, *J. Magn. Magn. Mater.* **133** (1994) 500.
12. M. I. ROSALES, A. M. PLATA, M. E. NICHO, A. BRITO, M. A. PONCE and V. M. CASTAÑO, *J. Mater. Sci.* **30** (1995) 4446.
13. A. MAKINO, Y. YAMATO and N. SAKATSUME, *J. Jpn Soc. Powder Powder Metall.* **39** (1992) 129.
14. S. KOMARNENI, E. FREGEAU, E. BREVAL and R. ROY, *J. Am. Ceram. Soc.* **71** (1988) C-26.
15. E. CEDILLO, J. OCAMPO, V. RIVERA and R. VALENZUELA, *J. Phys. E Sci. Instrum.* **13** (1980) 383.
16. A. GLOBUS, *Proc. J. Phys. Coll.* C1-38 (1977).
17. M. GUYOT and V. CAGAN, *J. Magn. Magn. Mater.* **27** (1982) 202.
18. V. G. HARRIS, M. C. KOON, C. M. WILLIAMS, Q. ZHANG, M. ABE and J. P. KIRKLAND, *IEEE Trans. Mag.* **31** (1995) pp 3473.
19. E. SCHLOEMANN, R. J. MAHER and J. A. WEISS, *ibid.* **31** (1995) 3470.
20. R. VALENZUELA, *J. Mater. Sci.* **15** (1980) 3173.
21. G. AGUILAR-SAHAGÚN, P. QUINTANA, E. AMANO, J. T. S. IRVINE and R. VALENZUELA, *J. Appl. Phys.* **75** (1994) 7000.
22. J. T. S. IRVINE, A. R. WEST, E. AMANO, A. HUANOSTA and R. VALENZUELA, *Sol. State Ionics* **40** (1990) 220.
23. M. I. ROSALES, E. AMANO, M. P. CUAUTLE and R. VALENZUELA, *J. Mater. Sci. Eng. B* **49** (1997) 221.
24. C. G. OLIVER, *IEEE Trans. Mag.* (1995) 3982.

Received 27 November 1996
and accepted 23 April 1998